Check for updates

Geobiology

WILEY

gebiology

ORIGINAL ARTICLE OPEN ACCESS

Microbially Enhanced Growth and Metal Capture by Ferromanganese Concretions in a Laboratory Experiment

Renata Majamäki[1] | Joonas Wasiljeff[1] | Lotta Purkamo[1] | Jenni Hultman[2,3] | Eero Asmala[1] | Pirjo Yli-Hemminki[2] | Kirsten S. Jørgensen[4] | Karoliina Koho[1] | Jukka Kuva[1] | Joonas J. Virtasalo[1]

[1]Geological Survey of Finland (GTK), Espoo, Finland | [2]Natural Resources Institute Finland (LUKE), Helsinki, Finland | [3]Department of Microbiology, University of Helsinki, Helsinki, Finland | [4]Finnish Environment Institute (SYKE), Helsinki, Finland

Correspondence: Renata Majamäki (renata.majamaki@gtk.fi)

Received: 18 June 2024 | **Revised:** 26 November 2024 | **Accepted:** 13 January 2025

Funding: This work was supported by Research Council of Finland and The Foundation for Research of Natural Resources in Finland (Grants 332249 and 20240020).

Keywords: Baltic Sea | biomineralization | ferromanganese | metal enrichment | microbial activity

ABSTRACT

The growth and metal enrichment of ferromanganese minerals on the seafloor have intrigued many studies, yet the role of microbes in the process has remained elusive. Here, we assessed the microbial influence on the growth and trace metal accumulation and release of ferromanganese concretions from the Baltic Sea using 12-week microcosm incubation experiments. We studied three concretion morphotypes: Crust, discoidal, and spheroidal, with biotic and abiotic treatments. The concretion samples were collected into bottles containing artificial brackish seawater from the Gulf of Finland, incubated in in-situ simulating conditions, and sampled at the beginning and end of the experiment. Microscale X-ray-computed tomography confirmed the local growth of up to 10 μm thick patches on the concretion surface during the 12-week incubation period, corresponding to a growth rate of 0.04 mm/year. Scanning electron microscopy of glass slides in the microcosms revealed freshly precipitated cauliflower-like grains, typical of freshly formed Fe- and Mn-hydroxides. Decreased concentrations of dissolved trace metals (Mn, Fe Co, V, Ni, Zn, and Mo) in the incubation solutions indicated the accumulation of these elements into concretions in the biotic microcosms. In contrast, the dissolution of concretions was observed in abiotic microcosms, confirming that microbial activity enhanced the ferromanganese precipitation and the associated accumulation and release of P and trace metals into the ambient solution. The microbial contribution was confirmed by a strong decrease in headspace methane concentrations in biotic microcosms, further indicating the presence of active methanotrophs in the concretion communities.

1 | Introduction

Ferromanganese (Fe—Mn) concretions are centimeter-scale accumulations of iron and manganese oxides forming at the sediment–water interface on the seafloor. The concretions are ubiquitous in oceans around the world and have been typically reported from deep-sea environments (e.g., Margolis and Burns 1976; Blöthe et al. 2015), freshwaters (e.g., Stein et al. 2001; Zemskaya et al. 2018; Schoettle and Friedman 1971), and also on the seafloor of the brackish Baltic Sea (e.g., Winterhalter 2004; Zhamoida et al. 1996; Wasiljeff et al. 2024). In the Gulf of Finland in the eastern Baltic Sea, concretions occur on the surface of soft clay and silt sediments with no or very low sediment net deposition (Winterhalter 2004). It has been estimated that more than 11% of the Finnish coastal sea areas are covered by concretion fields, located most abundantly in the Kvarken region of the Gulf of Bothnia and in the Gulf of Finland (Kaikkonen et al. 2019). The concretions have high contents of Fe and Mn and contain various other metals, such as Co, Ni, V, Zn,

This is an open access article under the terms of the Creative Commons Attribution License, which permits use, distribution and reproduction in any medium, provided the original work is properly cited.

© 2025 The Author(s). *Geobiology* published by John Wiley & Sons Ltd.

Mo, and rare earth elements (Zhamoida et al. 1996; Glasby et al. 1997), which make them potential resources of critical minerals (Ren et al. 2023).

In oxic seawater, Fe and Mn form complexes with organic compounds or precipitate as hydroxide particles that accumulate on the seafloor (Yu et al. 2015, 2024; Jilbert et al. 2018). This process is analogous to oceanic ferromanganese deposition enriched with metallic elements (Ren et al. 2022, 2024). The metal hydroxides can form ferromanganese concretions in seafloor areas where conditions are predominantly oxic and where there is no net sediment deposition, which is typical of the exposures of silty clays of the previous lacustrine phase of the Baltic Sea Basin (Zhamoida et al. 2017). The primary source of Fe and Mn in the Baltic Sea is terrestrial (Winterhalter 2004; Zhamoida et al. 1996). Additional Fe and Mn may be delivered to the site of ferromanganese precipitation by benthic efflux and lateral transport from nearby suboxic to anoxic sub-basins (Widerlund and Ingri 1996; Hlawatsch et al. 2002; Winterhalter 2004; Pakhomova et al. 2007), or by upward diffusion of porewater Fe and Mn from the underlying lacustrine sediment (Virtasalo and Kotilainen 2008). The enrichment of critical metals in Fe—Mn concretions is influenced by many factors, such as water depth, electrochemical speciation, post-depositional phosphatization, and nodule structural properties (Huang and Fu 2023). Metals are enriched with distinct pathways depending on the element. For instance, Co is scavenged on the Fe—Mn oxides through oxidation substitution, while Ni and Zn accumulate through direct complexation on the Mn oxides. It is suggested that Fe—Mn concretions are selectively enriched by oxidation-sensitive and high-field-strength elements from seawater (Ren et al. 2022, 2024), and elements are distributed between the Fe and Mn hydroxide phases (Ren et al. 2024). Some metals, such as Co and V, are correlated with Fe hydroxides, whereas Ni, Zn, and Mo are more closely linked to Mn hydroxides.

Furthermore, the concretions are occupied by diverse microbial communities with oxidative and reductive metabolism, influencing metal cycling (Ghiorse and Hirsch 1982; Yli-Hemminki, Jørgensen, and Lehtoranta 2014; Zhang et al. 2002; Sujith et al. 2017; Sujith and Gonsalves 2021). Previous studies have shown that concretions from the Baltic Sea are largely habited by species from phylum Pseudomonadota (previously Proteobacteria), including Mn- and Fe-oxidizers (e.g., Yli-Hemminki, Jørgensen, and Lehtoranta 2014; Reunamo et al. 2017), having thus potential to oxidize these elements and enhance the metal incorporation into concretions. In addition, many known methanotrophs that oxidize methane as an energy source belong to the Pseudomonadota (Hanson and Hanson 1996), suggesting that methanotrophs may be present in the Baltic Sea concretions.

Concretions occur in various shapes but can generally be categorized into three main morphotypes: Crust, discoidal, and spheroidal (Winterhalter 2004; Glasby et al. 1997; Zhamoida et al. 1996). Hydrodynamics and sedimentological conditions in the near-bottom seawater, such as the deposition rate and the position of a concretion in the sediment, influence the concretion shape (Zhamoida et al. 1996; Glasby et al. 1997; Wasiljeff et al. 2024). Consequently, the distribution of different morphotypes varies along the coastal area of Finland. These morphotypes also have distinct elemental compositions: Crust concretions are primarily rich in Fe, whereas spheroidal concretions are more Mn-rich, whereas discoidal concretions have a more mixed content of these elements (Zhamoida et al. 1996; Wasiljeff et al. 2024). Spheroidal concretions have the highest contents of magnetofossils produced by magnetotactic bacteria and the highest microbial mineralization rates (Wasiljeff et al. 2024). Furthermore, P is effectively adsorbed in concretions (Zhamoida et al. 2017; Hlawatsch et al. 2002; Winterhalter 2004) and functions as a natural sink for P, contributing to its cycling on the seafloor.

The growth rates of concretions on the Baltic Sea floor have been previously inferred based on various methods, such as concentrations of anthropogenic metals (Zhamoida et al. 1996), ^{210}Pb measurements (Grigoriev et al. 2013), and the ^{226}Ra/Ba$_{ex}$ ratio (Liebetrau et al. 2002), with rates ranging from 0.002 to 0.06 mm/year, depending on the method used and the morphotype of the studied concretion. In contrast, deep-sea nodules exhibit significantly slower growth rates, ranging from 1 to 5 mm/Myr (e.g., Hein and Koschinsky 2014; Ren et al. 2022), highlighting that concretions in the shallow Baltic Sea grow much faster than those in the deep sea. The accelerated growth rates in the Baltic Sea are attributed to enhanced microbial activity within the concretions (Ghiorse and Hirsch 1982; Yli-Hemminki, Jørgensen, and Lehtoranta 2014; Zhang et al. 2002; Zhamoida et al. 2007; Wasiljeff et al. 2024) and favorable conditions in the surrounding sediment (Winterhalter 1980).

This 12-week laboratory microcosm experiment investigated the concretion growth and incorporation of dissolved metals into natural Fe—Mn concretions collected from the Gulf of Finland. Specific focus is given to the influence of microbial activity, revealed through biotic and abiotic incubations and their role in both the sequestration and release of trace metals in the concretions. To gain insight into the similarities and dissimilarities between concretion morphotypes, we have chosen to investigate the three principal concretion morphotypes in the Baltic Sea: Crust, discoidal, and spheroidal.

2 | Materials and Methods

2.1 | Sampling and Study Sites

The artificial brackish seawater of the Gulf of Finland (salinity 4.7, Yli-Hemminki, Jørgensen, and Lehtoranta 2014; Table S1) was prepared and divided into 250 mL glass bottles containing 125 mL of artificial seawater before sampling. The initial pH of the artificial seawater was measured. All bottles and tools were acid-washed and sterilized in an autoclave.

Sediment samples with ferromanganese concretions on the surface were collected during two expeditions in May and June 2022 from the northern Gulf of Finland with a box corer (20 × 20 cm surface area) that was subsequently sampled onboard the research vessel Geomari of the Geological Survey of Finland (GTK) (Figure 1; Table 1). The samples were collected from three locations (later referred to as sites) that are known to contain all three main morphological types of concretions: Crust, discoidal, and spheroidal. Before the sampling, the seafloor coverage of the

14724669, 2025, 1, Downloaded from https://onlinelibrary.wiley.com/doi/10.1111/gbi.70010 by Luonnonvarakeskus, Wiley Online Library on [27/03/2026]. See the Terms and Conditions (https://onlinelibrary.wiley.com/terms-and-conditions) on Wiley Online Library for rules of use; OA articles are governed by the applicable Creative Commons License

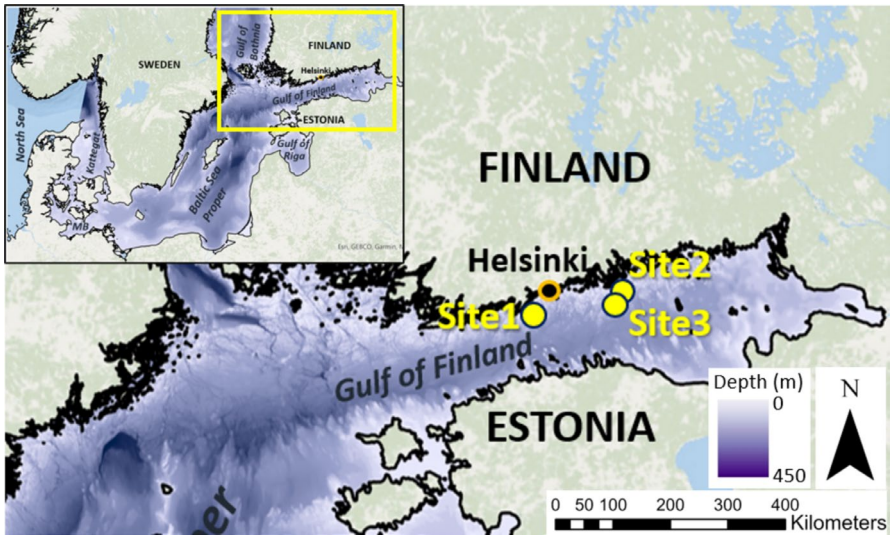

FIGURE 1 | Bathymetric map of the Baltic Sea with the study sites 1, 2, and 3 indicated. MB = Mecklenburg Bight. Base map: ESRI Inc. (Redlands) Ocean Basemap 2018. Baltic Sea bathymetric data: EMODnet Bathymetry 2018 (Thierry et al. 2019).

TABLE 1 | Geographical locations of study sites and the morphology of ferromanganese concretions collected from the Gulf of Finland.

Site	Sediment core ID	Latitude N (WGS84)	Longitude E (WGS84)	Date	Water depth (m)	Concretion morphology
1	MGBC-2022-1	59°57.941′	24°46.718′	6 May 2022	41	Crust
2	MGBC-2022-5	60°11.483′	26°01.895′	8 June 2022	30	Discoidal
3	MGBC-2022-7	60°05.493′	25°57.789′	8 June 2022	42	Spheroidal

concretions was confirmed with an underwater video camera. Water column temperature, salinity, and dissolved oxygen (DO) profiles were measured from each sampling site using a Sea & Sun Technology 90 M multiprobe.

To prepare microcosms, concretions were collected from the sediment sample surface and placed into the glass bottles containing 125 mL of artificial seawater using spoons and tweezers that were cleaned with 70% ethanol before and between samples. Before transferring the concretions into bottles, they were rinsed with filtered (nominal pore size 0.22 μm, polyethersulfone membrane) seawater to remove any excess fluffy (organic-rich material) and sediment from the concretions. The seawater was collected from a depth of 30 m using a Limnos water sampler, which was the maximum depth accessible with this sampler. The crust concretions were broken down into smaller pieces to fit into the bottles, whereas three to four individual discoidal and spheroidal concretions were placed into each bottle. The glass bottles with the concretions were stored in the dark at +8°C onboard the research vessel and directly transported to sample storage at +3.5°C at the GTK laboratory in Espoo at the end of each expedition.

2.2 | Microcosm Experiments

Three parallel incubation experiments were conducted, one for each concretion morphotype (Figure 2). Each incubation experiment was conducted using microcosm bottles capped with rubber septa: Three biotic microcosm bottles (biotic triplicates), one abiotic control obtained adding sodium azide (NaN_3) with a final concentration of 15 mM to eliminate microbial activity (Sujith et al. 2017), and two microcosm bottles dedicated to the assessment of concretion growth and freshly formed concretion material. Separate bottles were dedicated for the start (0 week) and the end of incubation (12 weeks). All microcosms were incubated in the dark at +3.5°C in an orbital shaker at 100 rpm to simulate seafloor conditions. Biotic triplicates and abiotic control were sacrificed, respectively, 2–3 days after collection (0 week) and after 12 weeks of incubation (12 weeks). Also, the duplicate microcosms, dedicated to the assessment of concretion growth and freshly formed concretion material, were sacrificed after 12 weeks of incubation, totalizing 10 microcosm bottles per experiment. From 0 week and 12 weeks microcosms (biotic triplicates and abiotic control), the pH of the incubation solution was measured, and the headspace methane concentrations and total phosphorus (total-P) and metal concentrations of the incubation solutions were analyzed as described in Section 2.4.

To assess the growth or the dissolution of single concretions, an approximately millimetric piece of concretion was attached to the end of a glass rod and scanned with X-ray computed tomography (CT) as described in Section 2.3. After CT scanning, the other end of the glass rod was attached to the rubber septum capping the microcosm bottle, so that the concretion piece was immersed in the artificial seawater, incubated for 12 weeks as described above, and scanned again with CT after 12 weeks of incubation.

14724669, 2025, 1, Downloaded from https://onlinelibrary.wiley.com/doi/10.1111/gbi.70010 by Luonnonvarakeskus, Wiley Online Library on [27/03/2026]. See the Terms and Conditions (https://onlinelibrary.wiley.com/terms-and-conditions) on Wiley Online Library for rules of use; OA articles are governed by the applicable Creative Commons License

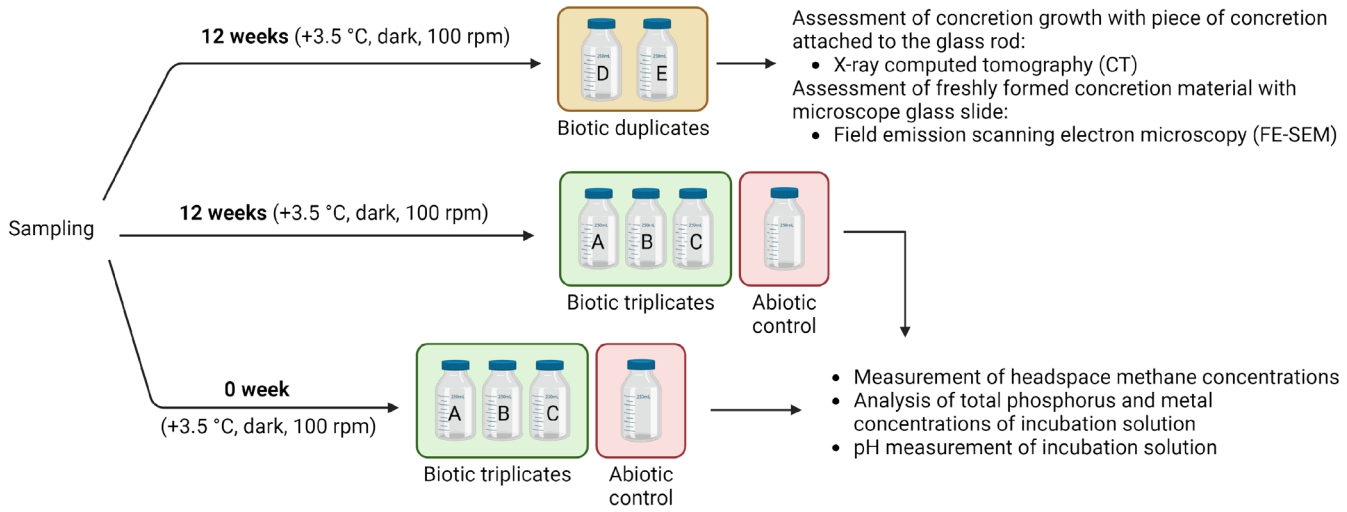

FIGURE 2 | Design and workflow of microcosm experiment per sampling site. Three parallel series of incubations for each concretion morphotype were conducted, and a total of 10 microcosm bottles were dedicated for each incubation experiment per site. A, B, C = biotic triplicates, D, E = biotic duplicates with a concretion piece attached to the glass rod and a microscope glass slide.

In addition, a freshly formed concretion material was assessed by placing a clean microscope glass slide into the same duplicate incubation bottles containing the glass rods with the concretion pieces. After the 12-week incubation, the surfaces of the microscope glass slides were air-dried and pressed with a conductive carbon tape. The tapes were coated with Au and scanned using a field emission scanning electron microscope as described in Section 2.3.

2.3 | X-Ray Computed Tomography and Field Emission Scanning Electron Microscopy

The piece of concretion, attached to the end of a glass rod, was scanned with a GE Phoenix v|tome|x s at the GTK using a 180 kV nanofocus tube in focus mode 2 (small) with no beam filter. The accelerating voltage was 100 kV, and the tube current was 260 µA for a total power of 26 W. 2700 projections were taken during a 360°C rotation. At every angle, the detector waited for a single exposure time and then took an average of three exposures. With a single exposure time of 2000 ms, the total scan time per sample was 6 h. The obtained resolutions were 1.27–1.45 µm depending on the sample. The images were reconstructed with Phoenix datos|x 2 using a ring artefact reduction but no beam-hardening correction. The CT scanning was repeated after 12 weeks of incubation with the same settings, including resolution. The CT images were analyzed using ThermoFisher PerGeos 2020.2. The images taken before and after the 12 weeks of incubation were overlaid on top of each other using the Register images tool, which is very robust in 3D-3D registration. They were then subtracted from each other to highlight the growth areas. As the growth patches were quite local, their thicknesses were measured using the measure distance tool for perpendicular cross sections to get a coarse estimate for local thickness increase.

The particles on the carbon tapes were analyzed via a field emission scanning electron microscope, model JEOL JSM-7100F Schottky equipped with an Oxford Instrument EDS-spectrometer X-Max 80 mm^2 (SDD). The secondary electron (SE) images and the EDS point analyses were taken using a 15 kV acceleration voltage and a 1.0 nA probe current. The analyses were taken using Aztec software. The quality of the EDS analysis is semi-quantitative, and the results are normalized to 100%. Be and lighter elements are not possible to detect.

2.4 | Geochemical Analysis

To analyze methane concentrations, the headspace was sampled from 0-week and 12-week microcosm bottles and introduced into 20 mL pre-evacuated gas-tight glass vials using a needle and syringe through the bottles' rubber caps and stored at +3.5°C until analysis (Figure 2). Headspace methane concentrations (CH_4) were measured with an Agilent 7890B gas chromatograph (GC; Agilent Technologies, Santa Clara, CA, USA) with a flame ionization detector (FID) equipped with a Gilson GX271 autosampler.

To assess the metal concentrations of the incubation solution, 100 mL of solution from each bottle was filtered through a 0.2 µm cellulose acetate filter and stored at +3.5°C in plastic bottles with a final concentration of 4.5% (v/v) of nitric acid (HNO_3) until analysis. In addition, 100 mL of artificial seawater was stored in the plastic bottle described above to define the initial composition of the incubation solution. Solutions were measured at Hellabs, University of Helsinki, Finland, using an Agilent 8900 triple quadrupole ICP-MS (ICP-QQQ) system to assess the concentrations of total-P, Fe, Mn Co, Ni, V, Zn, and Mo. These elements were chosen for this study because they are common components of ferromanganese concretions as well as essential trace metals for microbial metabolism. The samples were analyzed in accordance with ISO 17294-2:2016. Matrix interferences were handled using He, H_2, O_2, and no-gas tuning modes and TDS matrix suppression using HMI. Data quality control was performed using surface water reference materials SPS-SW2 (Spectrapure Standards, Norway) and TM23-5 (ECCC, Canada), along with the soft drinking water reference material LGC6027 (LGC Ltd., United

14724669, 2025, 1, Downloaded from https://onlinelibrary.wiley.com/doi/10.1111/gbi.70010 by Luonnonvarakeskus, Wiley Online Library on [27/03/2026]. See the Terms and Conditions (https://onlinelibrary.wiley.com/terms-and-conditions) on Wiley Online Library for rules of use; OA articles are governed by the applicable Creative Commons License

Kingdom). Each reference material was individually adjusted to match the acidity of the sample matrix, achieved through the addition of HNO_3 and/or dilution as necessary. Certified reference material concentrations for total P, Fe, Mn Co, Ni, V, Zn, and Mo are presented in Table S2. The detection limits in μg/L were 0.06 (total-P), 0.08 (Fe), 0.01 (Mn), 0.01 (Co), 0.02 (Ni), 0.01 (V), 0.03 (Zn), and 0.03 (Mo).

The figures were created by normalizing concentrations with the measured values of artificial seawater (Figure 7; Table S4). The concentration differences between the 0-week and 12-week incubations were expressed as the relative change by subtracting the 0-week values from the 12-week values and dividing by the 0-week value (Figure 7, upper panels; Table S7). Original concentrations for total-P, Fe, Mn Co, Ni, V, Zn, and Mo are presented in Table S5.

3 | Results

3.1 | Vertical Profiles of Temperature, DO, Salinity and pH, and Occurrence of Fe—Mn Concretions

At all the sampling sites, the seawater temperature and dissolved oxygen (DO) concentration decreased with depth, while salinity increased (Figure 3). At site 1, the temperature and DO concentration decreased downward in the water column and were ca. +2°C and 9 mL/L, respectively, at the bottom. Salinity increased downward and reached a maximum of 6.8 at the bottom. At site 2, the temperature decreased to ca. +4°C, and DO concentration decreased to 8.3 mL/L at the bottom. The salinity increased to 5.5 at the bottom. At site 3, the temperature was +3°C, DO concentration was 4.5 mL/L

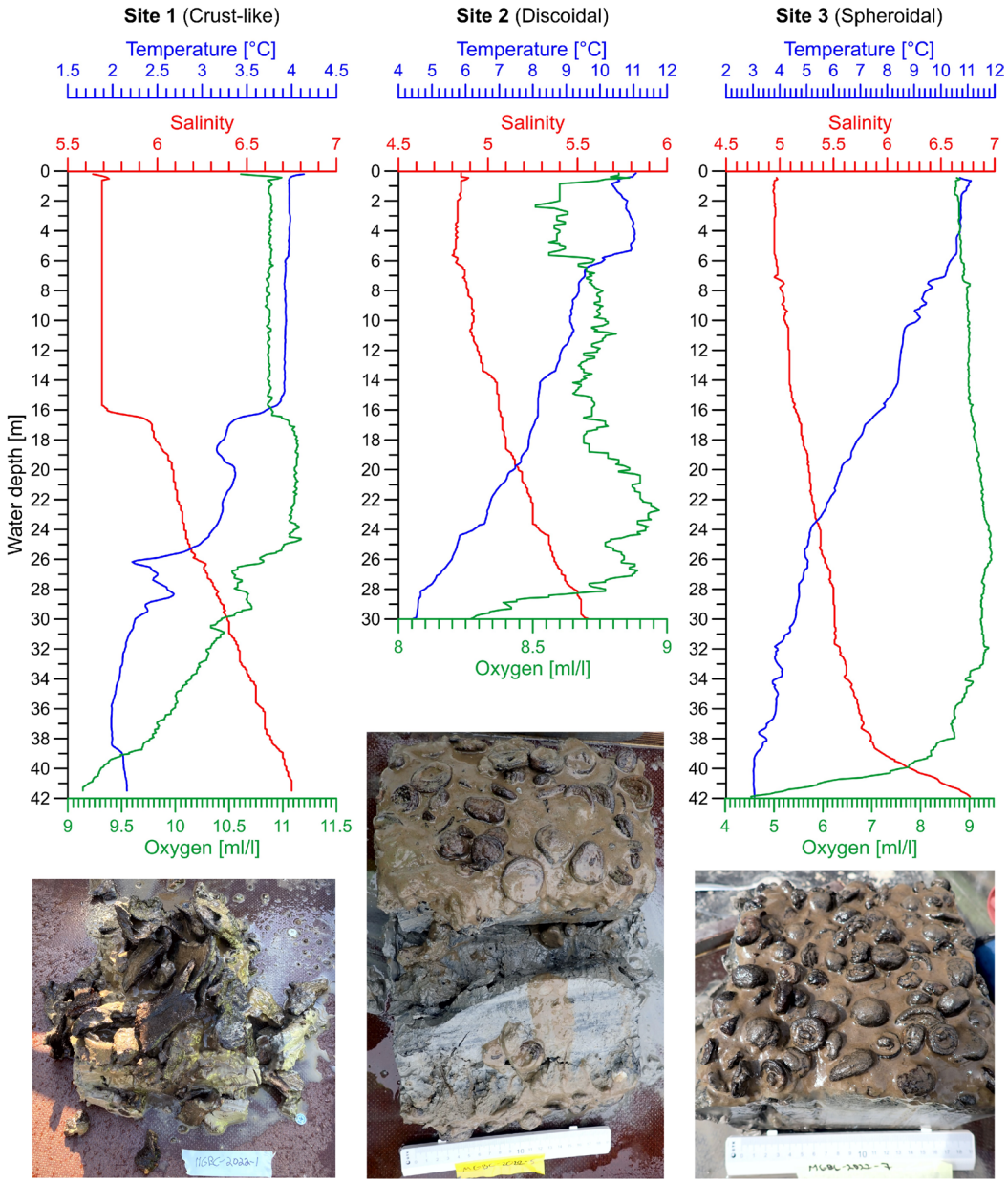

FIGURE 3 | Depth profiles of temperature, dissolved oxygen concentration and salinity, and collected sediment cores with ferromanganese concretions on their surface from the three study sites. Site 1 was characterized by crust concretions, site 2 by discoidal concretions, and site 3 by discoidal and spheroidal concretions. Only spheroidal concretions were collected from site 3.

14724669, 2025, 1, Downloaded from https://onlinelibrary.wiley.com/doi/10.1111/gbi.70010 by Luonnonvarakeskus, Wiley Online Library on [27/03/2026]. See the Terms and Conditions (https://onlinelibrary.wiley.com/terms-and-conditions) on Wiley Online Library for rules of use; OA articles are governed by the applicable Creative Commons License

at the bottom. Salinity increased at the bottom, reaching 6.8. The pH values at the bottom were 6.8, 7.6, and 8.1 at sites 1, 2, and 3, respectively.

Ferromanganese concretions occurred as a ca. 1.5 cm thick surface layer in each sediment sample (Figure 3). The concretions were covered by a fluffy, brownish organic-rich material. The sediment underlying the concretions was gray glaciolacustrine rhythmite silt and clay at site 1, while it was Fe-monosulfide-banded gray postglacial lacustrine silty clay at site 2 (sediment identification follows Virtsalo et al. 2007; Virtasalo, Hämäläinen, and Kotilainen 2014). At site 3, the concretions were underlain by a 2 cm thick Fe-monosulfide-darkened fine sand, which in turn was sharply underlain by brownish-gray glaciolacustrine rhythmite silt and clay.

3.2 | Changes in pH and Headspace Methane Concentrations in Microcosm Experiments

The artificial seawater had an initial pH of 6.9. In microcosms, the pH of the incubation solution ranged in biotic triplicates from 6.5 to 7.4 and in abiotic controls from 6.5 to 7.5 (Table 2). The pH of the incubation solution of the site 1 microcosms was not measured at 0 week but only after 12 weeks of incubation. In site 2, the pH decreased by an average of 0.5 units in the biotic triplicates after 12 weeks of incubation, while a small increase (by 0.1) was observed in the abiotic control. In site 3, the pH increased by an average of 0.2 units in the biotic triplicates and by 0.3 units in abiotic control after 12 weeks of incubation.

In biotic triplicates and abiotic controls from all three sites, the headspace methane (CH_4) concentrations were lower after the 12-week incubation than after the 0-week incubation (Figure 4; Table S3). In biotic triplicates, methane concentrations decreased more than that in the abiotic controls. In the site 1 biotic triplicates, the methane concentration decreased the most, and the mean CH_4 concentration was 55% lower (1.97 ± 0.07 ppm) in the 12-week incubation (1.62 ± 0.06 ppm) than in the 0-week incubation (3.60 ± 0.09 ppm). In the site 2 biotic triplicates, the mean CH_4 concentration was 38% lower (1.35 ± 0.11 ppm) in the 12-week incubation (2.20 ± 0.08 ppm) than in the 0-week incubation (3.55 ± 0.14 ppm). In the site 3 biotic triplicates, CH_4 concentration was 28% lower (0.99 ± 0.12 ppm) in the 12-week incubation (2.59 ± 0.14 ppm) than in the respective 0-week

TABLE 2 | pH values of the incubation solution from biotic triplicates and abiotic control at the beginning and end of 12 weeks of incubation from three different sites. The 0-week pH values from site 1 samples were not measured.

	Site 1 (crust)	Site 2 (discoidal)		Site 3 (spheroidal)	
Biotic triplicates	12-week	0-week	12-week	0-week	12-week
A	7.4	7.3	6.7	6.5	6.7
B	7.1	7.0	6.5	6.6	6.9
C	7.4	7.0	6.6	6.9	7.1
Mean (STD)	7.3 (0.14)	7.1 (0.14)	6.6 (0.08)	6.7 (0.17)	6.9 (0.16)
Abiotic control	7.5	6.7	6.8	6.5	6.8

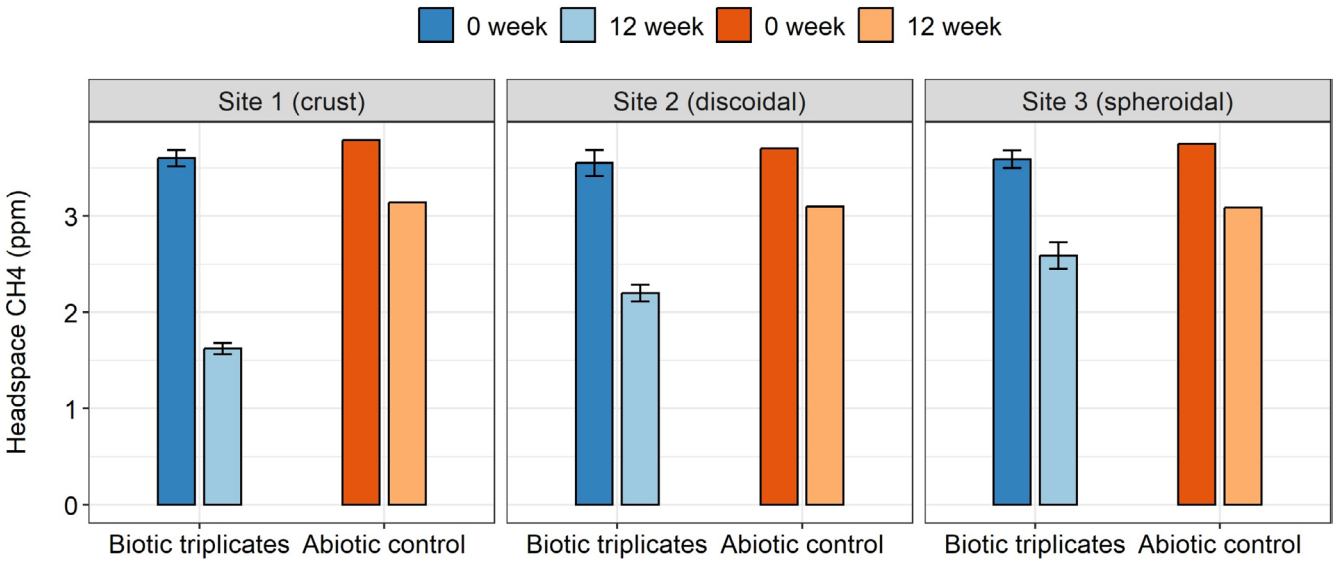

FIGURE 4 | Mean headspace methane concentrations in the 0-week and 12-week microcosms from three sites. Error bars show the standard deviations of the biotic triplicates. See Table S3 for original values.

14724669, 2025, 1, Downloaded from https://onlinelibrary.wiley.com/doi/10.1111/gbi.70010 by Luonnonvarakeskus, Wiley Online Library on [27/03/2026]. See the Terms and Conditions (https://onlinelibrary.wiley.com/terms-and-conditions) on Wiley Online Library for rules of use; OA articles are governed by the applicable Creative Commons License

incubation (3.59 ± 0.09 ppm). The decrease in the headspace methane concentrations in the abiotic controls was approximately 17% on each site.

3.3 | Concretion Growth in CT and FE-SEM-EDS Examination

Overlay CT images, where a 0-week image was subtracted from a 12-week image, revealed that precipitation had occurred on the surface of the ferromanganese concretion pieces (Figure 5). The growth was detected locally on the crust and spheroidal morphotypes from site 1 and site 3. The new growth was visible as bright patches along the concretion surface, and the local thickness increase varied depending on the concretion morphotype. The mean local increase in both crust and spheroidal morphotypes was 5.5 μm in thickness (range from 4 to 10 μm) and 100 μm in width (range from 50 to 200 μm) in 12 weeks.

In site 1, the freshly precipitated Fe—Mn material was observed in two areas (areas A and B; Figure 5) on the concretion surface. In area A, the new growth was visible along the whole surface. The mean local thickness increase calculated from four (I–IV) selected patches was 5.4 μm, ranging from 3.7 μm to 7.1 μm (patch thicknesses: I, 7.1 μm; II, 4.8 μm; III, 3.7 μm; and IV, 6.1 μm). In area B, the new growth was visible as 50–100 μm wide patches on the concretion surface, and the mean local thickness increase from three (I–III) selected patches was 5.9 μm, ranging from 3.5 μm up to 10.1 μm (patch thicknesses: I, 10.1 μm; II, 3.5 μm; and III, 4.2 μm). In site 3, the freshly precipitated Fe—Mn material was detected along the surface as a 200 μm wide patch. The mean local thickness increase from three (I-III) selected points was 5.2 μm, ranging from 4.2 μm to 6.2 μm (patch thickness: I, 4.2 μm; II, 5.2 μm; and III, 6.2 μm).

FE-SEM imaging revealed that mineral material was attached to the glass slides during the 12-week incubation. The applied carbon tapes contained small mineral grains, including Fe hydroxides (Figure 6a). The Fe-hydroxide grains typically had diameters of less than 10 μm and cauliflower-like morphologies. The EDS analyses were focused on the tips of cauliflower-shaped buds and showed compositions dominated by O, Mn, and Fe (Figure 6b).

3.4 | Total Phosphorus and Metal Concentrations in the Incubation Solutions

In all microcosms from each sampling site, the dissolved metal concentrations of the incubation solution increased more in the abiotic controls than in the biotic triplicates after the 12-week incubation (Figure 7). In site 1 biotic triplicates, mean Fe, Co, V, Zn, and Mo concentrations decreased after 12 weeks of incubation, while the mean P, Mn, and Ni concentrations of the 12-week incubation were slightly higher than that of the 0-week incubation (Figure 7a). In contrast, in the abiotic control, the 12-week microcosms had substantially higher Mn, Fe Co, and Ni concentrations than the 0-week microcosms, while the difference was small for P, V, Zn, and Mo concentrations.

Sites 2 and 3 microcosms revealed consistent behavior of dissolved metal concentrations in the solutions (Figure 7b,c). The mean Mn, Fe Co, Ni, V, Zn, and Mo concentrations of biotic triplicates were systematically lower in the 12-week incubation than in the 0-week incubation. In contrast, in the abiotic controls, these concentrations were higher in the 12-week incubation, but Fe concentration was lower in both sites and V and Zn concentrations were lower in site 2. The differences in P concentration were small between the 0-week and 12-week incubation in both the biotic triplicates and abiotic controls.

There was a high variability between biotic triplicates, and the error bars of standard deviation are thus not presented in the figures presenting the differences between 0-week and 12-week incubation (Figure 7a–c upper panel; Table S7).

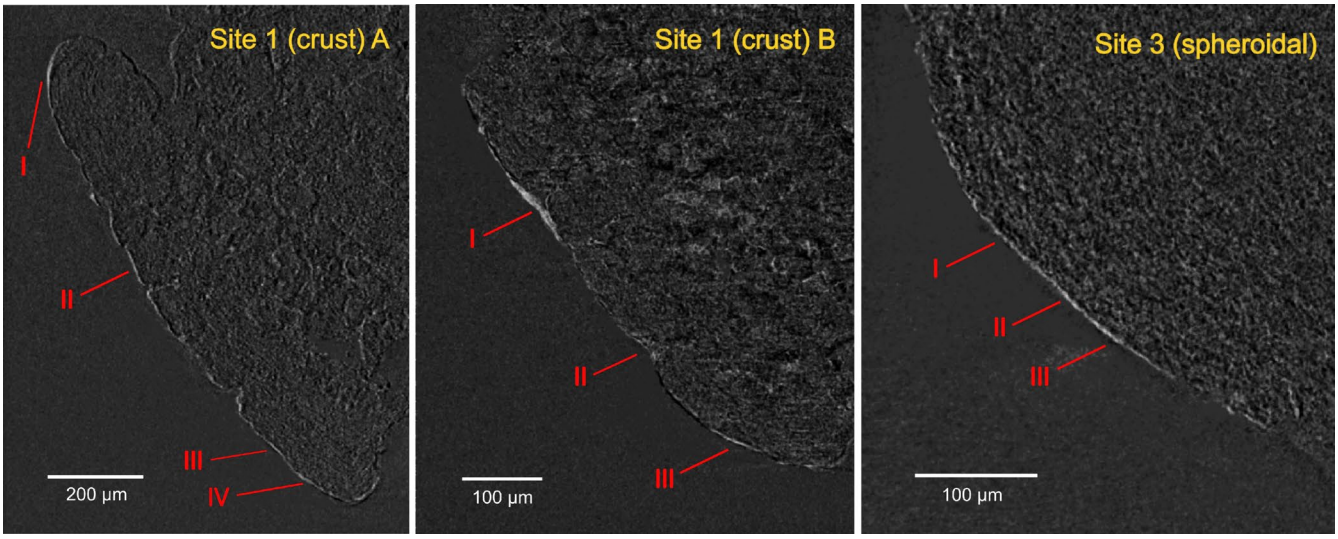

FIGURE 5 | Overlay CT images from the 12 weeks of incubation at site 1 (areas A and B) and site 3 show freshly precipitated ferromanganese material as bright patches on the concretion surface. Roman numerals (I–IV) indicate fresh ferromanganese patches, as discussed in the text.

14724669, 2025, 1, Downloaded from https://onlinelibrary.wiley.com/doi/10.1111/gbi.70010 by Luonnonvarakeskus, Wiley Online Library on [27/03/2026]. See the Terms and Conditions (https://onlinelibrary.wiley.com/terms-and-conditions) on Wiley Online Library for rules of use; OA articles are governed by the applicable Creative Commons License

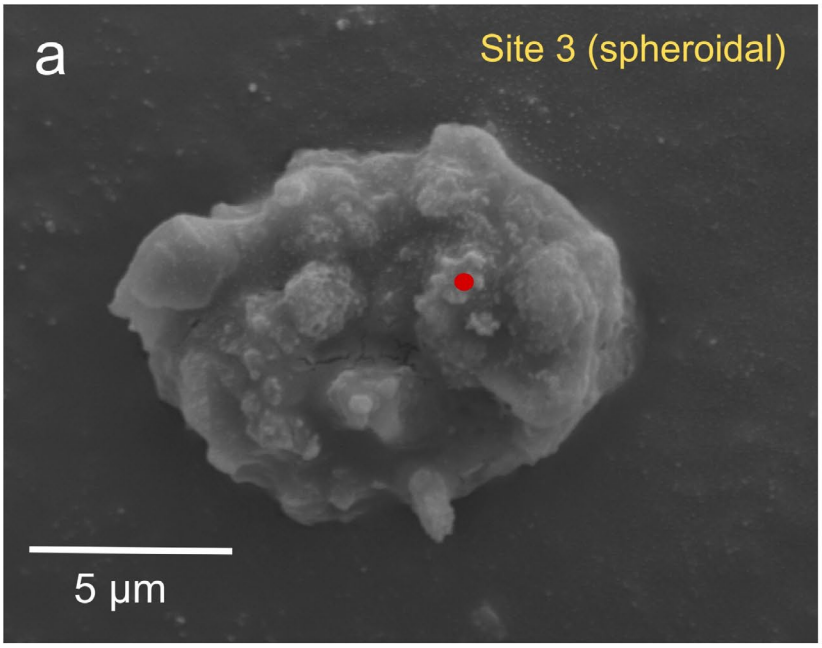

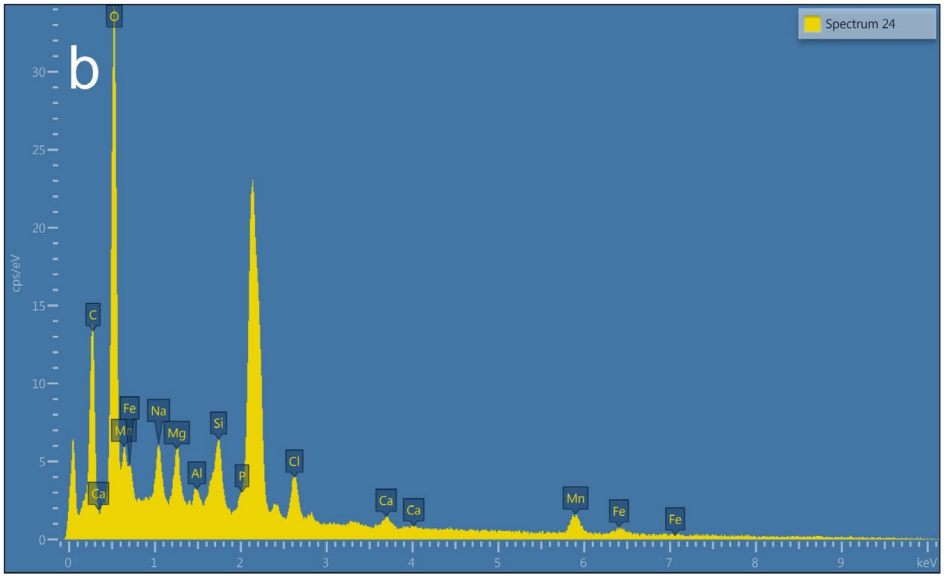

Element	Weight %
O	32.36
Mn	24.81
Fe	17.94
Cl	10.37
Na	6.62
Mg	3.57
Ca	1.55
Si	1.46

FIGURE 6 | (a) SEM image and (b) EDS spectrum of a ferromanganese grain on the site 3 glass slide after the 12-week incubation. The EDS spectrum was measured from the location indicated by the red dot in the SEM image. Weight % values lower than 1% have been excluded from the table.

4 | Discussion

This study documents, for the first time to our knowledge, the growth of ferromanganese concretions in a laboratory microcosm experiment.

We collected the concretions from the northern Gulf of Finland, where temperature, salinity, and dissolved oxygen at the three study sites had typical values for the area: The ranges of near-bottom water temperature (2°C–4°C) and salinity (5.5–6.8) fit within the regional and temporal variabilities (Alenius, Myrberg, and Nekrasov 1998; Figure 3). Additionally, the near-bottom water pH showed typical values (6.8–8.1) at the sites. In the Gulf of Finland, the surface seawater pH ranges from 7.67 to 8.51, depending on the season, whereas the near-bottom water pH is usually lower due to respiration (HELCOM 2023). The concretions form through the oxidation of dissolved Fe and Mn, which requires oxygen-rich conditions (Winterhalter 1980; Zhamoida et al. 1996; Hlawatsch et al. 2002). In this study, the near-bottom water at sites 1 and 2 was well-oxygenated (9.1 and 8.3 mL/L DO, respectively), while the DO concentration at site 3 was slightly lower (4.5 mL/L) yet still considered well-oxygenated (approx. 50% of saturation) and sufficient for Fe and Mn to precipitate (Hlawatsch et al. 2002; Sutherland et al. 2020; Callender and Bowser 1976). The concretions occurred as ca. 1.5 cm thick layer on the seafloor, covering the exposed old fine-grained sediments from the previous lacustrine phase of the Baltic Sea Basin, which have lower organic matter contents than the reducing organic-rich mud that is being deposited today in nearby areas in the brackish water Baltic Sea (Virtsalo et al. 2007; Virtasalo, Hämäläinen, and Kotilainen 2014). Sediment distribution on the coastal seafloor is patchy; roughly, a third is composed of

14724669, 2025, 1, Downloaded from https://onlinelibrary.wiley.com/doi/10.1111/gbi.70010 by Luonnonvarakeskus, Wiley Online Library on [27/03/2026]. See the Terms and Conditions (https://onlinelibrary.wiley.com/terms-and-conditions) on Wiley Online Library for rules of use; OA articles are governed by the applicable Creative Commons License

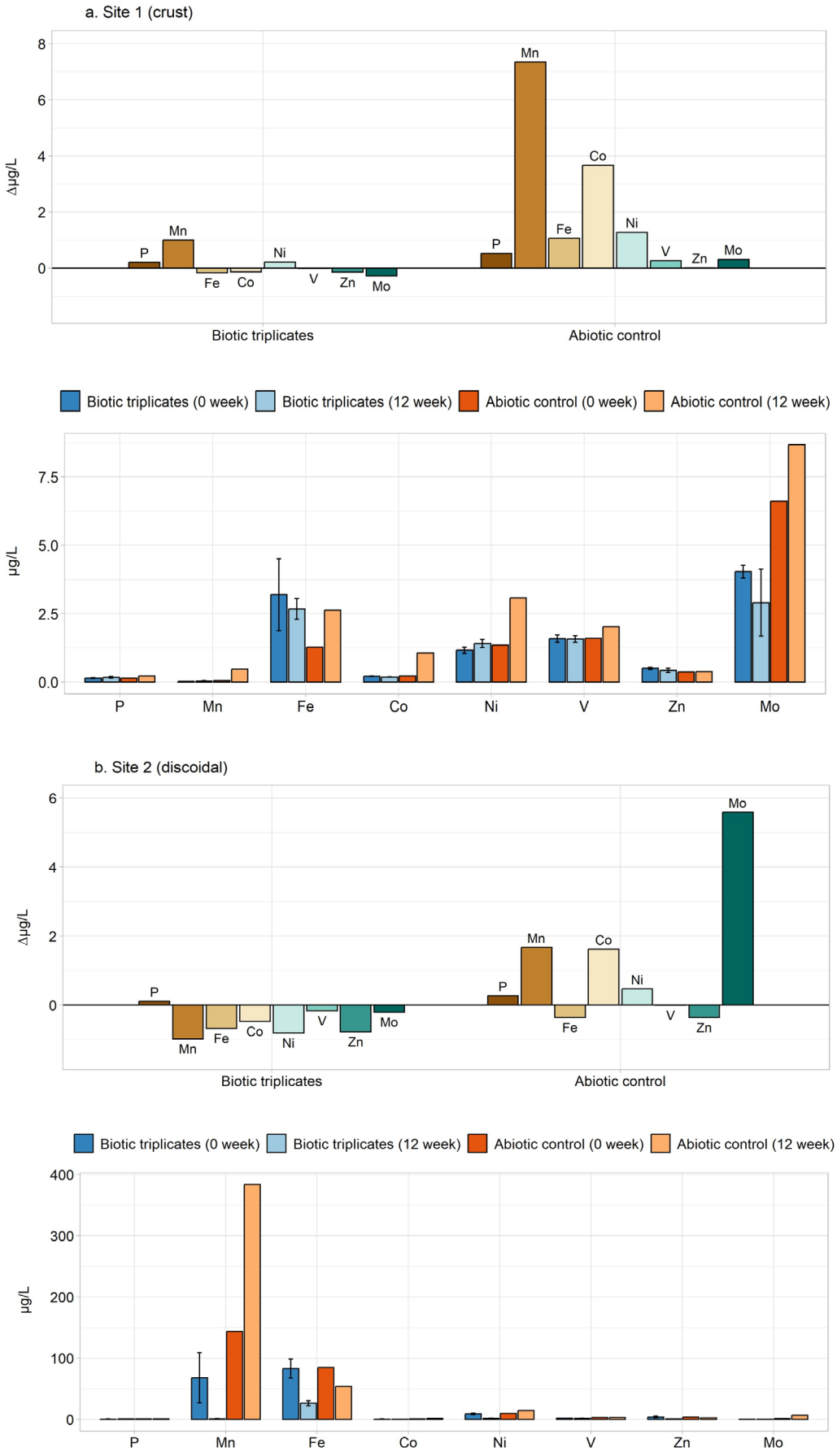

FIGURE 7 | (Continued)

14724669, 2025, 1, Downloaded from https://onlinelibrary.wiley.com/doi/10.1111/gbi.70010 by Luonnonvarakeskus, Wiley Online Library on [27/03/2026]. See the Terms and Conditions (https://onlinelibrary.wiley.com/terms-and-conditions) on Wiley Online Library for rules of use; OA articles are governed by the applicable Creative Commons License

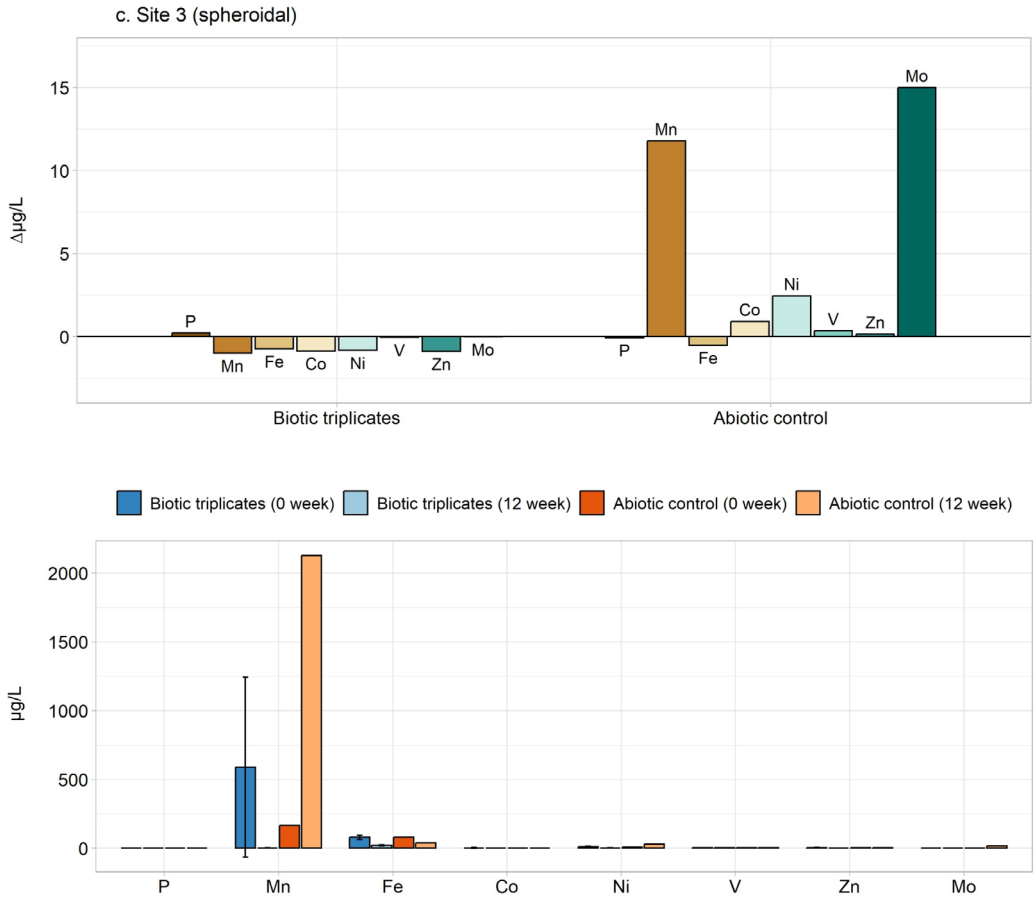

FIGURE 7 | Mean concentrations of P, Mn, Fe Co, Ni, V, Zn, and Mo in the solutions of biotic triplicates and abiotic control in 0-week and 12-week incubation (lower panel; Table S6) and the concentration differences between the 0-week and 12-week incubation (upper panel; Table S7) in (a) site 1, (b) site 2, and (c) site 3. In the upper panels, bars with positive values have labels above them, while bars with negative values have labels below them. The concentrations are normalized with the measured values of artificial seawater (Table S4). The concentration differences are expressed as the relative change by subtracting the 0-week values from the 12-week values and dividing by the 0-week value. Error bars show the standard deviation of the biotic triplicates. See Table S5 for original concentrations.

glaciolacustrine and postglacial lacustrine silty clay, a third of organic-rich brackish-water mud, and a third of bedrock and till. At all three sampling sites, the conditions were thus favorable for forming and preserving ferromanganese concretions that require oxic seafloor conditions and no net sediment deposition (Winterhalter 1980, 2004; Zhamoida et al. 1996).

X-ray CT revealed freshly precipitated ferromanganese material on the surface of the concretions after the 12-week microcosm experiments (Figure 5). The thickest growth of up to 10 μm was observed for a patch on a crust concretion from site 1. This 10 μm local thickness increase corresponds to a growth rate of 0.04 mm/year, which is close to the previously estimated growth rates from the Baltic Sea, based on the analyses of transects over cross sections of concretions. In the Gulf of Finland, Zhamoida et al. (1996) estimated average growth rates of 0.03–0.06 mm/year for spheroidal concretions based on the increased concentrations of metals (Cu, Ni, and Zn) in the outer layers of concretions, whereas Grigoriev et al. (2013) estimated average growth rate of 0.014 mm/year for the same morphotype based on ^{210}Pb isotope measurements. In Mecklenburg Bay in the southwestern Baltic Sea, Liebetrau et al. (2002) estimated growth rates of 0.0017–0.021 mm/year for spheroidal and crust morphotypes based on the $^{226}Ra_{ex}$/Ba method. The concretions of the comparably shallow Baltic Sea grow notably faster than the deep-sea nodules, whose growth rates have been estimated to be on average of 1–5 mm/Myr analyzed with Be, U, and Os isotopes (Hein and Koschinsky 2014), although a faster growth rate of 168 mm/Myr for a deep-sea Mn nodule in the Pacific has been documented (Reyss, Marchig, and Ku 1982). The rapid growth rate of Baltic Sea concretions is explained by the relatively high availability of Fe and Mn and favorable conditions on the seafloor. The large rivers Neva and Kymi deliver high concentrations of Fe and Mn to the Gulf of Finland (Zhamoida et al. 1996; Leivuori 1998), which to significant extent are transported and deposited on the seafloor as metal hydroxides (Yu et al. 2015, 2024; Jilbert et al. 2018). In addition, the typical substrate of ferromanganese occurrences in the region, the patchily exposed silty clay of the previous lake phase of the Baltic Sea Basin, and its underlying glacial till contain abundant reactive Fe and Mn minerals that are dissolved in porewater (Callender and Bowser 1976; Virtasalo and Kotilainen 2008). Fe and Mn are also imported by benthic efflux and lateral transport from nearby areas with reducing organic-rich mud of the modern brackish-water Baltic Sea (Widerlund and Ingri 1996; Hlawatsch et al. 2002; Winterhalter 2004; Pakhomova et al. 2007). Finally, enhanced microbial activity within concretions has been

14724669, 2025, 1, Downloaded from https://onlinelibrary.wiley.com/doi/10.1111/gbi.70010 by Luonnonvarakeskus, Wiley Online Library on [27/03/2026]. See the Terms and Conditions (https://onlinelibrary.wiley.com/terms-and-conditions) on Wiley Online Library for rules of use; OA articles are governed by the applicable Creative Commons License

associated with their rapid growth (Ghiorse and Hirsch 1982; Yli-Hemminki, Jørgensen, and Lehtoranta 2014; Zhang et al. 2002; Zhamoida et al. 2007; Wasiljeff et al. 2024).

Ferromanganese particles that were observed on the glass slides during the 12-week incubation were generally smaller than 10 μm and exhibited irregular and cauliflower-like morphologies, typical for freshly formed Fe- and Mn-hydroxides (Figure 6). Similar cauliflower-like morphologies have previously been documented for deep-sea ferromanganese samples (Karpoff et al. 2017; Usui et al. 2020) and in a laboratory experiment (Cheng et al. 2014). However, it cannot be ruled out that a piece of concretion could have detached from the concretion and reattached to the glass slide surface during incubation.

The removal of dissolved metals from the solution of biotic triplicates during the 12-week incubation suggests that these metals were incorporated into the newly precipitated ferromanganese material (Figure 7a–c). In contrast, the increased dissolved metal concentrations in the abiotic controls imply the release of metals into the solution and the dissolution of concretions in the absence of microbial communities. Enhanced metal incorporation into Fe—Mn concretions in biotic triplicates shows that the microbial community has a strong control on the metal accumulation, consistent with previous studies that indicate that microbes contribute to the formation of concretions (e.g., Ghiorse and Hirsch 1982; Yli-Hemminki, Jørgensen, and Lehtoranta 2014; Zhang et al. 2002; Sujith et al. 2017; Sujith and Gonsalves 2021).

The formation of Fe—Mn concretions is a complex biogeochemical process (Glasby et al. 1997; Hlawatsch et al. 2002; Winterhalter 2004) in which microbes play a role by directly or indirectly oxidizing dissolved Fe and Mn from the sediment porewater and near-bottom seawater. The concretions in the Baltic Sea are predominantly hosted by species belonging to the phylum Pseudomonadota (previously Proteobacteria) (e.g., Yli-Hemminki, Jørgensen, and Lehtoranta 2014; Reunamo et al. 2017). This metabolically diverse phylum includes many Mn- and Fe-oxidizers (Tebo et al. 2005; Hedrich, Schlömann, and Johnson 2011; Madigan et al. 2018), suggesting their potential role in the oxidation of both elements. Mn-oxidizing bacteria, *Sphingomonas, Pseudomonas*, and *Bacillus* were identified in the concretions of the Gulf of Finland (Yli-Hemminki, Jørgensen, and Lehtoranta 2014) and Mn-oxidizers *Bacillus, Arthrobacter*, and *Pseudomonas* were dominant in biofilms found on crusts from the Pacific Ocean (Jiang et al. 2017). Fe-oxidizers, *Hyphomicrobiaceae* and *Scalinduaceae*, were discovered in fast-growing Arctic Fe—Mn nodules from the Kara Sea (Shulga et al. 2022). In addition to Fe and Mn, microbes influence the availability and cycling of other metals, such as Co, Ni, V, Zn, and Mo, by utilizing them for cell functions and altering their oxidation states. Microbes actively uptake metals that are required as cofactors in enzymes to catalyze various reactions (Madigan et al. 2018; Cavet et al. 2015). For instance Co is essential for vitamin B12 synthesis (Dereven'kov et al. 2016; Raux, Schubert, and Warren 2000), while Mo can be a cofactor for the nitrate reductase enzyme (Johnson, Hainline, and Rajagopalan 1980). Furthermore, by altering the oxidation states of metals, microbes can promote metal enrichment into Fe—Mn concretions (Sujith et al. 2017; Sujith and Gonsalves 2021). For instance, Mn-oxidizing bacteria can directly catalyze Co(II) oxidation to Co(III) (Lee and Tebo 1994). Alternatively, Co can undergo indirect oxidation through the biogenic formation of Mn oxides by Mn-oxidizers where Co(II) is subsequently adsorbed onto Mn oxides and further oxidized to Co(III) by Mn(IV) (Murray and Dillard 1979; Burns 1976), finally enhancing the Co(III) enrichment into Mn oxides.

In our microcosm experiments, discoidal and spheroidal concretions (Sites 2 and 3) had the strongest precipitation rates (Figure 7b,c), which suggests relatively high microbial activity in these morphotypes. Previously, the spheroidal concretions in the Baltic Sea have been associated with enhanced bacterial activity based on increased contents of magnetofossils that are produced by magnetotactic bacteria and higher microbial biomineralization rate (Wasiljeff et al. 2024). Notable dissolution rates were observed in the abiotic controls in all sites, especially with Co in crust morphotype (Site 1) and Mo in discoidal and spheroidal morphotypes (Sites 2 and 3). Co and Mo can be bound to both Fe- and Mn-rich phases in ferromanganese concretions (Kashiwabara et al. 2013; Huang and Fu 2023) and an increase in Fe content may lead to enhanced scavenging of Co (Zhang, Liu, and Zhao 2023). The Co content is further associated with the growth speed of the concretions and is thus coupled to the Fe/Mn ratio (Takahashi et al. 2007). Given that the Fe-rich crust concretions generally form slower than the Mn-rich discoidal and spheroidal morphotypes (e.g., Wasiljeff et al. 2024; our data), the different dissolved Co and Mo contents might reflect these relationships in the abiotic controls. The P was released into solution in the abiotic controls in all sites, yet a small release was also observed in the biotic triplicates. The observed effect was contrary to expectations, as the surface metal oxides in ferromanganese concretions typically adsorb dissolved P, contributing to its cycling and sequestration (Hlawatsch et al. 2002; Winterhalter 2004; Zhamoida et al. 2017). It is worth noting that NaN_3, used for inhibiting microbial activity in abiotic controls, can reduce dissolved Fe (II) to Fe (Hendrix et al. 2019). However, the reaction is relatively fast, taking place in minutes. The 0-week microcosms were sampled 3–4 days after the addition of NaN_3, when the reaction of NaN_3 with Fe (II) must have been largely completed. Therefore, the effect of NaN_3 addition on Fe geochemistry is likely minimal and similar in both 0-week and 12-week microcosms.

0-Week biotic triplicates from sites 2 and 3 displayed elevated concentrations of Fe and strongly elevated concentrations of Mn in the incubation solutions, whereas site 1 showed only a slightly elevated Fe concentration (Figure 7, lower panels). Ferromanganese concretions typically contain amorphous and poorly crystalline Fe and Mn oxide phases, including ferrihydrite, goethite, and birnessite-like minerals (e.g., Zhamoida et al. 1996; Post 1999; Marcus, Manceau, and Kersten 2004; Baturin 2009), that can readily adsorb aqueous Fe and Mn species (e.g., Hiemstra and van Riemsdijk 2007; Lefkowitz and Elzinga 2017). The elevated Fe and Mn levels observed at the initial stage of the experiment likely resulted from the desorption of these surface-adsorbed Fe and Mn complexes

14724669, 2025, 1, Downloaded from https://onlinelibrary.wiley.com/doi/10.1111/gbi.70010 by Luonnonvarakeskus, Wiley Online Library on [27/03/2026]. See the Terms and Conditions (https://onlinelibrary.wiley.com/terms-and-conditions) on Wiley Online Library for rules of use; OA articles are governed by the applicable Creative Commons License

due to interfacial redox reactions and minor changes in pH and temperature during and shortly after the introduction of the concretion material into the incubation solution. The discoidal and spheroidal concretions (Sites 2 and 3) may have had higher contents of surface-adsorbed Mn and Fe, which were released into the solution at the beginning of the incubation experiment. In contrast, this effect was smaller in the crust concretions (Site 1), which is consistent with the morphotype generally having high Fe and low Mn contents. The higher surface-adsorbed contents may be linked to the higher microbial activities in sites 2 and 3, which were inferred based on the stronger decreases in dissolved metal concentrations in the 12-week incubations compared to site 1. Alternatively, the higher adsorbed Fe and Mn contents in discoidal and spheroidal concretions may have resulted in the higher Fe and Mn availability, resulting in stronger ferromanganese precipitation during the experiment. The concentration of Fe was initially low in the artificial brackish seawater (Table S4) before the start of the incubation experiment, indicating that Fe had partially dissolved prior to the experiments. The decrease in the pH in the solution of biotic triplicates was expected due to microbial respiration and the production of carbonic acid into the solution, yet surprisingly, a small increase in pH was observed in the spheroidal concretion morphotype (Table 2). Nevertheless, the pH remaining relatively stable and nearly neutral in all microcosms indicates that the metals did not dissolve due to acidic conditions. The solubility of many metals increases as the pH decreases, e.g. Fe in oxidizing waters below a pH of 5 (Hem 1985), and thus, acidic conditions can induce the release of metals from concretions.

We calculate that a 2 μg/L decrease in the Fe concentration of the solution equals the precipitation of 190,000 μm^3 of fresh Fe hydroxide (density 4.25 g/cm^3, porosity 50%) in the microcosm, and a similar decrease in the Mn concentration equals to the precipitation of 250,000 μm^3 of fresh Mn hydroxide (density 3.26 g/cm^3, porosity 50%) in the microcosm. These estimates are conservative as concentration changes of up to tens and hundreds of μg/L were noted (Figure 7), but they demonstrate that the decreases in Fe and Mn concentrations in the biotic triplicates are sufficient to precipitate the newly formed Fe—Mn patches observed in the CT images that are generally smaller than 52,000 μm^3.

The headspace methane concentrations decreased more in biotic triplicates with microbial communities than in abiotic controls (Figure 4). This suggests that the decrease in headspace methane concentrations was driven by microbial activity, likely attributed to methanotrophic bacteria that utilize methane oxidation as an energy source (Hanson and Hanson 1996). We detected the highest rate of methane utilization (55%) in the crust concretion from site 1, suggesting that this morphotype has the most active methanotrophic communities. The observed small decrease in methane concentrations of abiotic controls (approx. 17% in all sites) may be due to the relatively low concentration of NaN_3 (15 mM) and the long incubation time, which may have allowed minor microbial activity during incubation (Cabrol, Quéméneur, and Misson 2017). Alternatively, NaN_3 may have had a direct impact on ionic strength, affecting the solubility of methane.

Since the study sites in our experiment were well-oxygenated and the microcosms remained oxic during incubation, we suggest that aerobic methanotrophs were responsible for the methane decrease. Previous studies have shown that Pseudomonadota were predominant in the Baltic Sea Fe—Mn concretions (Yli-Hemminki, Jørgensen, and Lehtoranta 2014; Reunamo et al. 2017), and this phylum includes many known methanotrophs. While the current knowledge of the aerobic methanotrophs in the Baltic Sea concretions is limited, aerobic methane oxidizers have been previously documented in sediments. Aerobic methanotrophs, *Methylococcales*, *Methylocystaceae*, and *Ca. Methylacidiphilum sp.*, were found in the surface sediments of estuaries in southwest Finland, suggesting aerobic methane oxidation (Myllykangas et al. 2020). In addition, a small number of *Methylococcales* were identified in the surface sediment layers of the Western Gulf of Finland (Broman et al. 2020), and in sediments surrounding Fe—Mn concretions in Lake Baikal, southern Siberia (Zemskaya et al. 2018). However, the microbial communities in concretions and surrounding sediments can distinct from each other (Tully and Heidelberg 2013; Wu et al. 2013), and therefore the involvement of aerobic methanotrophs in the Baltic Sea concretions requires further investigation.

5 | Conclusions

We documented the growth of ferromanganese concretions during 12-week microcosm experiments by microscale computed tomography and loss of metals from the incubation solution. The observed mean local thickness increase of patches on the concretion surface was 5.5 μm for the crust and spheroidal morphotype, while the highest local thickness increase was up to 10 μm in 12 weeks for the crust morphotype, corresponding to a growth rate of 0.04 mm/year. In addition, we documented ferromanganese grains up to 10 μm in diameter precipitated during the incubation experiment. Dissolved metal concentrations decreased in the biotic treatments, indicating the capture of trace metals into concretions due to microbial activity. The highest precipitation rate of metals was detected in spheroidal and discoidal morphotypes, suggesting elevated microbial activity in these morphotypes. The microbially enhanced growth and metal accumulation of the studied concretions highlight the important role of microbes in the biogeochemical cycling of metals in the Baltic Sea ecosystems.

Acknowledgments

This research was funded by the Finnish Natural Resources Research Foundation (grant no. 20240020) and the Research Council of Finland (grant no. 332249 Fermaid). This study has used research facilities provided by the Finnish Marine Research Infrastructure (FINMARI) network. We thank the captains and crews of RV Geomari for their help with sediment core sampling. XCT was funded by the Research Council of Finland via the RAMI infrastructure project (#293109). We acknowledge Sari Lukkari for the assistance with FE-SEM-EDS imagining and analysis at the Geological Survey of Finland, Espoo. We thank Juhani Virkanen for ICP-MS measurements at the HelLabs (HelLabs publication #0027), University of Helsinki, and Heini Ali-Kovero for GC measurements at the Faculty of Biological and Environmental Sciences, University of Helsinki.

14724669, 2025, 1, Downloaded from https://onlinelibrary.wiley.com/doi/10.1111/gbi.70010 by Luonnonvarakeskus, Wiley Online Library on [27/03/2026]. See the Terms and Conditions (https://onlinelibrary.wiley.com/terms-and-conditions) on Wiley Online Library for rules of use; OA articles are governed by the applicable Creative Commons License

Conflicts of Interest

The authors declare no conflicts of interest.

Data Availability Statement

The data that supports the findings of this study are available in the Supporting Information of this article.

References

Alenius, P., K. Myrberg, and A. Nekrasov. 1998. "The Physical Oceanography of the Gulf of Finland: A Review." *Boreal Environment Research* 3: 97–125.

Baturin, G. N. 2009. "Geochemistry of Ferromanganese Nodules in the Gulf of Finland, Baltic Sea." *Lithology and Mineral Resources* 44: 411–426. https://doi.org/10.1134/S0024490209050010.

Blöthe, M., A. Wegorzewski, C. Müller, F. Simon, T. Kuhn, and A. Schippers. 2015. "Manganese-Cycling Microbial Communities Inside Deep-Sea Manganese Nodules." *Environmental Science & Technology* 49: 7692–7700. https://doi.org/10.1021/es504930v.

Broman, E., X. Sun, C. Stranne, et al. 2020. "Low Abundance of Methanotrophs in Sediments of Shallow Boreal Coastal Zones With High Water Methane Concentrations." *Frontiers in Microbiology* 11: 1536–1536. https://doi.org/10.3389/fmicb.2020.01536.

Burns, R. G. 1976. "The Uptake of Cobalt Into Ferromanganese Nodules, Soils, and Synthetic Manganese (IV) Oxides." *Geochimica et Cosmochimica Acta* 40, no. 1: 95–102. https://doi.org/10.1016/0016-7037(76)90197-6.

Cabrol, L., M. Quéméneur, and B. Misson. 2017. "Inhibitory Effects of Sodium Azide on Microbial Growth in Experimental Resuspension of Marine Sediment." *Journal of Microbiological Methods* 133: 62–65. https://doi.org/10.1016/j.mimet.2016.12.021.

Callender, E., and C. J. Bowser. 1976. "Freshwater Ferromanganese Deposits." In *Handbook of Strata-Bound and Stratiform Ore Deposits*, edited by K. H. Wolf, Au, U, Fe, Mn, Hg, Sb, W, and P Deposits, 341–394. Amsterdam: Elsevier. https://doi.org/10.1016/B978-0-444-41407-6.50011-8.

Cavet, J. S., R. D. Perry, S. Brunke, et al. 2015. "Chapter 7—Trace Metals in Host–Microbe Interactions: The Microbe Perspective." In *Trace Metals and Infectious Diseases*, edited by J.O. Nriagu and E. P. Skaar, pp. 99. Cambridge: MIT Press. https://doi.org/10.7551/mitpress/9780262029193.003.0010.

Cheng, X.-L., J.-S. Jiang, C.-Y. Jin, C.-C. Lin, Y. Zeng, and Q.-H. Zhang. 2014. "Cauliflower-Like α-Fe_2O_3 Microstructures: Toluene–Water Interface-Assisted Synthesis, Characterization, and Applications in Wastewater Treatment and Visible-Light Photocatalysis." *Chemical Engineering Journal* 236: 139–148. https://doi.org/10.1016/j.cej.2013.09.089.

Dereven'kov, I. A., D. S. Salnikov, R. Silaghi-Dumitrescu, S. V. Makarov, and O. I. Koifman. 2016. "Redox Chemistry of Cobalamin and Its Derivatives." *Coordination Chemistry Reviews* 309: 68–83. https://doi.org/10.1016/j.ccr.2015.11.001.

Ghiorse, W. C., and P. Hirsch. 1982. "Isolation and Properties of Ferromanganese-Depositing Budding Bacteria From Baltic Sea Ferromanganese Concretions." *Applied and Environmental Microbiology* 43: 1464–1472. https://doi.org/10.1128/aem.43.6.1464-1472.1982.

Glasby, G. P., E. M. Emelyanov, V. A. Zhamoida, et al. 1997. "Environments of Formation of Ferromanganese Concretions in the Baltic Sea: A Critical Review." *Geological Society Special Publication* 119: 213–237. https://doi.org/10.1144/GSL.SP.1997.119.01.14.

Grigoriev, A. G., V. A. Zhamoida, K. A. Gruzdov, and R. S. Krymsky. 2013. "Age and Growth Rates of Ferromanganese Concretions From the Gulf of Finland Derived From 210Pb Measurements." *Oceanology* 53: 345–351. https://doi.org/10.1134/S0001437013030041.

Hanson, R. S., and T. E. Hanson. 1996. "Methanotrophic Bacteria." *Microbiological Reviews* 60: 439–471. https://doi.org/10.1128/MMBR.60.2.439-471.1996.

Hedrich, S., M. Schlömann, and D. B. Johnson. 2011. "Iron-Oxidizing Proteobacteria." *Microbiology (Society for General Microbiology)* 157, no. Pt 6: 1551–1564. https://doi.org/10.1099/mic.0.045344-0.

Hein, J. R., and A. Koschinsky. 2014. "13.11—Deep-Ocean Ferromanganese Crusts and Nodules." In *Treatise on Geochemistry*, edited by H. D. Holland and K.K. Turekian. Second ed., 273–291. Oxford: Elsevier Ltd. https://doi.org/10.1016/B978-0-08-095975-7.01111-6.

HELCOM. 2023. "Baltic Sea Acidification." HELCOM element indicator report. https://indicators.helcom.fi/indicator/acidification/.

Hem, J. D. 1985. *Study and Interpretation of the Chemical Characteristics of Natural Water.* Report. 3rd ed Water-Supply Paper, Series: 2254. U.S. Geological Survey, Reston, VA: USGS. https://doi.org/10.3133/wsp2254.

Hendrix, K., N. Bleyen, T. Mennecart, C. Bruggeman, and E. Valcke. 2019. "Sodium Azide Used as Microbial Inhibitor Caused Unwanted By-Products in Anaerobic Geochemical Studies." *Applied Geochemistry* 107: 120–130. https://doi.org/10.1016/j.apgeochem.2019.05.014.

Hiemstra, T., and W. H. van Riemsdijk. 2007. "Adsorption and Surface Oxidation of Fe(II) on Metal (Hydr)oxides." *Geochimica et Cosmochimica Acta* 71: 5913–5933. https://doi.org/10.1016/j.gca.2007.09.030.

Hlawatsch, S., T. Neumann, C. M. G. van den Berg, M. Kersten, J. Harff, and E. Suess. 2002. "Fast-Growing, Shallow-Water Ferro-Manganese Nodules From the Western Baltic Sea: Origin and Modes of Trace Element Incorporation." *Marine Geology* 182: 373–387. https://doi.org/10.1016/S0025-3227(01)00244-4.

Hlawatsch, S., C. D. Garbe-Schönberg, F. Lechtenberg, et al. 2002. "Trace Metal Fluxes to Ferromanganese Nodules From the Western Baltic Sea as a Record for Long-Term Environmental Changes." *Chemical Geology* 182: 697–709. https://doi.org/10.1016/S0009-2541(01)00346-1.

Huang, S., and Y. Fu. 2023. "Enrichment Characteristics and Mechanisms of Critical Metals in Marine Fe–Mn Crusts and Nodules: A Review." *Minerals (Basel)* 13: 1532. https://doi.org/10.3390/min13121532.

Jiang, X.-D., X.-M. Sun, Y. Guan, et al. 2017. "Biomineralisation of the Ferromanganese Crusts in the Western Pacific Ocean." *Journal of Asian Earth Sciences* 136: 58–67. https://doi.org/10.1016/j.jseaes.2017.01.025.

Jilbert, T., E. Asmala, C. Schröder, et al. 2018. "Impacts of Flocculation on the Distribution and Diagenesis of Iron in Boreal Estuarine Sediments." *Biogeosciences* 15: 1243–1271. https://doi.org/10.5194/bg-15-1243-2018.

Johnson, J. L., B. E. Hainline, and K. V. Rajagopalan. 1980. "Characterization of the Molybdenum Cofactor of Sulfite Oxidase, Xanthine, Oxidase, and Nitrate Reductase. Identification of a Pteridine as a Structural Component." *Journal of Biological Chemistry* 255, no. 5: 1783–1786. https://doi.org/10.1016/S0021-9258(19)85945-8.

Kaikkonen, L., E. A. Virtanen, K. Kostamo, J. Lappalainen, and A. T. Kotilainen. 2019. "Extensive Coverage of Marine Mineral Concretions Revealed in Shallow Shelf Sea Areas." *Frontiers in Marine Science* 6. https://doi.org/10.3389/fmars.2019.00541.

Karpoff, A. M., D. Sauter, M. Cannat, M. Ulrich, and G. Manatschal. 2017. "Fe-Si Oxides Tracing the Ongoing Low-T° Hydrothermal Alteration of Exhumed Serpentinites at the Ultraslow-Spreading Southwest Indian Ridge." *Procedia Earth and Planetary Science* 17: 280–283. https://doi.org/10.1016/j.proeps.2016.12.055.

Kashiwabara, T., Y. Takahashi, M. A. Marcus, et al. 2013. "Tungsten Species in Natural Ferromanganese Oxides Related to Its Different Behavior From Molybdenum in Oxic Ocean." *Geochimica et Cosmochimica Acta* 106: 364–378. https://doi.org/10.1016/j.gca.2012.12.026.

14724669, 2025, 1, Downloaded from https://onlinelibrary.wiley.com/doi/10.1111/gbi.70010 by Luonnonvarakeskus, Wiley Online Library on [27/03/2026]. See the Terms and Conditions (https://onlinelibrary.wiley.com/terms-and-conditions) on Wiley Online Library for rules of use; OA articles are governed by the applicable Creative Commons License

Lee, Y., and B. M. Tebo. 1994. "Cobalt(II) Oxidation by the Marine Manganese(II)-Oxidizing Bacillus sp. Strain SG-1." *Applied and Environmental Microbiology* 60, no. 8: 2949–2957. https://doi.org/10.1128/AEM.60.8.2949-2957.1994.

Lefkowitz, J. P., and E. J. Elzinga. 2017. "Structural Alteration of Hexagonal Birnessite by Aqueous Mn(II): Impacts on Ni(II) Sorption." *Chemical Geology* 466, no. C: 524–532. https://doi.org/10.1016/j.chemgeo.2017.07.002.

Leivuori, M. 1998. "Heavy Metal Contamination in Surface Sediments in the Gulf of Finland and Comparison With the Gulf of Bothnia." *Chemosphere (Oxford)* 36, no. 1: 43–59. https://doi.org/10.1016/S0045-6535(97)00285-3.

Liebetrau, V., A. Eisenhauer, N. Gussone, G. Wörner, B. T. Hansen, and T. Leipe. 2002. "226 ra Excess /Ba Growth Rates and U-Th-Ra-Ba Systematic of Baltic Mn/Fe Crusts." *Geochimica et Cosmochimica Acta* 66: 73–83. https://doi.org/10.1016/S0016-7037(01)00766-9.

Madigan, M. T., K. S. Bender, D. H. Buckley, W. M. Sattley, and D. A. Stahl. 2018. "Chapter 3: Microbial Metabolism." In *Brock Biology of Microorganisms* (Global edition), edited by M.T Madigan, K. S. Bender, D. H. Buckley, W. M. Sattley, and D. A. Stahl. Unit 1, 111. Harlow, United Kingdom: Pearson Education.

Marcus, M. A., A. Manceau, and M. Kersten. 2004. "Mn, Fe, Zn and as Speciation in a Fast-Growing Ferromanganese Marine Nodule." *Geochimica et Cosmochimica Acta* 68: 3125–3136. https://doi.org/10.1016/j.gca.2004.01.015.

Margolis, S. V., and R. G. Burns. 1976. "Pacific Deep-Sea Manganese Nodules: Their Distribution, Composition, and Origin." *Annual Review of Earth and Planetary Sciences* 4: 229–263. https://doi.org/10.1146/annurev.ea.04.050176.001305.

Murray, J. W., and J. G. Dillard. 1979. "The Oxidation of Cobalt(II) Adsorbed on Manganese Dioxide." *Geochimica et Cosmochimica Acta* 43, no. 5: 781–787. https://doi.org/10.1016/0016-7037(79)90261-8.

Myllykangas, J.-P., A. J. Rissanen, S. Hietanen, and T. Jilbert. 2020. "Influence of Electron Acceptor Availability and Microbial Community Structure on Sedimentary Methane Oxidation in a Boreal Estuary." *Biogeochemistry* 148: 230–291. https://doi.org/10.1007/s10533-020-00660-z.

Pakhomova, S. V., P. O. J. Hall, M. Y. Kononets, A. G. Rozanov, A. Tengberg, and A. V. Vershinin. 2007. "Fluxes of Iron and Manganese Across the Sediment–Water Interface Under Various Redox Conditions." *Marine Chemistry* 107, no. 3: 319–331. https://doi.org/10.1016/j.marchem.2007.06.001.

Post, J. E. 1999. "Manganese Oxide Minerals: Crystal Structures and Economic and Environmental Significance." *Proceedings of the National Academy of Sciences of the United States of America* 96: 3447–3454. https://doi.org/10.1073/pnas.96.7.3447.

Raux, E., H. L. Schubert, and M. J. Warren. 2000. "Biosynthesis of Cobalamin (Vitamin B12): A Bacterial Conundrum." *Cellular and Molecular Life Sciences: CMLS* 57, no. 13–14: 1880–1893. https://doi.org/10.1007/pl00000670.

Ren, J., G. He, X. Deng, et al. 2022. "Metallogenesis of Co-Rich Ferromanganese Nodules in the Northwestern Pacific: Selective Enrichment of Metallic Elements From Seawater." *Ore Geology Reviews* 143: 104778. https://doi.org/10.1016/j.oregeorev.2022.104778.

Ren, J., G. He, Y. Yang, et al. 2024. "Ultraselective Enrichment of Trace Elements in Seawater by co-Rich Ferromanganese Nodules." *Global and Planetary Change* 239: 104498. https://doi.org/10.1016/j.gloplacha.2024.104498.

Ren, J., H. Yao, Y. Yang, et al. 2023. "Critical Metal Enrichment in Atypical Hydrogenetic Ferromanganese Nodules: A Case Study in the Central Basin Ridge of the West Philippine Basin." *Chemical Geology* 615: 121224. https://doi.org/10.1016/j.chemgeo.2022.121224.

Reunamo, A., P. Yli-Hemminki, J. Nuutinen, J. Lehtoranta, and K. S. Jørgensen. 2017. "Degradation of Crude Oil and PAHs in Iron-Manganese Concretions and Sediment From the Northern Baltic Sea." *Geomicrobiology Journal* 34: 385–399. https://doi.org/10.1080/01490451.2016.1197987.

Reyss, J. L., V. Marchig, and T. L. Ku. 1982. "Rapid Growth of a Deep-Sea Manganese Nodule." *Nature (London)* 295, no. 5848: 401–403. https://doi.org/10.1038/295401a0.

Schoettle, M., and G. M. Friedman. 1971. "Fresh Water Iron-Manganese Nodules in Lake George, New York." *Geological Society of America Bulletin* 82: 101–109. https://doi.org/10.1130/0016-7606(1971)82[101:FWINIL]2.0.CO;2.

Shulga, N., S. Abramov, A. Klyukina, K. Ryazantsev, and S. Gavrilov. 2022. "Fast-Growing Arctic Fe–Mn Deposits From the Kara Sea as the Refuges for Cosmopolitan Marine Microorganisms." *Scientific Reports* 12, no. 1: 21916–21967. https://doi.org/10.1038/s41598-022-23449-6.

Stein, L. Y., M. T. La Duc, T. J. Grundl, and K. H. Nealson. 2001. "Bacterial and Archaeal Populations Associated With Freshwater Ferromanganous Micronodules and Sediments." *Environmental Microbiology* 3: 10–18. https://doi.org/10.1046/j.1462-2920.2001.00154.x.

Sujith, P. P., and M. J. B. D. Gonsalves. 2021. "Ferromanganese Oxide Deposits: Geochemical and Microbiological Perspectives of Interactions of Cobalt and Nickel." *Ore Geology Reviews* 139: 104458. https://doi.org/10.1016/j.oregeorev.2021.104458.

Sujith, P. P., D. Ramanan, M. J. B. D. Gonsalves, and P. A. LokaBharathi. 2017. "Microbial Activity Promotes the Enrichment of Cobalt Over Nickel on Hydrogenetic Ferromanganese Crusts." *Marine Georesources & Geotechnology* 35: 1158–1167. https://doi.org/10.1080/1064119X.2017.1298169.

Sutherland, K. M., J. A. G. Wostbrock, C. M. Hansel, Z. D. Sharp, J. R. Hein, and S. D. Wankel. 2020. "Ferromanganese Crusts as Recorders of Marine Dissolved Oxygen." *Earth and Planetary Science Letters* 533: 116057. https://doi.org/10.1016/j.epsl.2019.116057.

Takahashi, Y., A. Manceau, N. Geoffroy, M. A. Marcus, and A. Usui. 2007. "Chemical and Structural Control of the Partitioning of Co, Ce, and Pb in Marine Ferromanganese Oxides." *Geochimica et Cosmochimica Acta* 71: 984–1008. https://doi.org/10.1016/j.gca.2006.11.016.

Tebo, B. M., H. A. Johnson, J. K. McCarthy, and A. S. Templeton. 2005. "Geomicrobiology of Manganese(II) Oxidation." *Trends in Microbiology (Regular ed.)* 13, no. 9: 421–428. https://doi.org/10.1016/j.tim.2005.07.009.

Thierry, S., S. Dick, S. George, L. Benoit, and P. Cyrille. 2019. "EMODnet Bathymetry a Compilation of Bathymetric Data in the European Waters." In *OCEANS 2019—Marseille*, 1–7. France: IEEE. https://doi.org/10.1109/OCEANSE.2019.8867250.

Tully, B. J., and J. F. Heidelberg. 2013. "Microbial Communities Associated With Ferromanganese Nodules and the Surrounding Sediments." *Frontiers in Microbiology* 4: 161–161. https://doi.org/10.3389/fmicb.2013.00161.

Usui, A., H. Hino, D. Suzushima, et al. 2020. "Modern Precipitation of Hydrogenetic Ferromanganese Minerals During On-Site 15-Year Exposure Tests." *Scientific Reports* 10: 3558–3558. https://doi.org/10.1038/s41598-020-60200-5.

Virtasalo, J. J., J. Hämäläinen, and A. T. Kotilainen. 2014. "Toward a Standard Stratigraphical Classification Practice for the Baltic Sea Sediments: The CUAL Approach." *Boreas* 43: 924–938. https://doi.org/10.1111/bor.12076.

Virtasalo, J. J., and A. T. Kotilainen. 2008. "Phosphorus Forms and Reactive Iron in Lateglacial, Postglacial and Brackish-Water Sediments of the Archipelago Sea (Northern Baltic Sea)." *Marine Geology* 252: 1–12.

Virtsalo, J. J., A. T. Kotilainen, M. E. Räsänen, and A. E. K. Ojala. 2007. "Late-Glacial and Post-Glacial Deposition in a Large, Low Relief,

14724669, 2025, 1, Downloaded from https://onlinelibrary.wiley.com/doi/10.1111/gbi.70010 by Luonnonvarakeskus, Wiley Online Library on [27/03/2026]. See the Terms and Conditions (https://onlinelibrary.wiley.com/terms-and-conditions) on Wiley Online Library for rules of use; OA articles are governed by the applicable Creative Commons License

Epicontinental Basin: The Northern Baltic Sea." *Sedimentology* 54: 1323–1344. https://doi.org/10.1111/j.1365-3091.2007.00883.x.

Wasiljeff, J., J. M. Salminen, A. P. Roberts, et al. 2024. "Morphology-Dependent Magnetic Properties in Shallow-Water Ferromanganese Concretions." *Geochemistry, Geophysics, Geosystems* 25. https://doi.org/10.1029/2023GC011366.

Widerlund, A., and J. Ingri. 1996. "Redox Cycling of Iron and Manganese in Sediments of the Kalix River Estuary, Northern Sweden." *Aquatic Geochemistry* 2: 185–201. https://doi.org/10.1007/BF00121631.

Winterhalter, B. 1980. "Ferromanganese Concretions in the Baltic Sea." In *Geology and Geochemistry of Manganese*, edited by L. M. Varentsov and G. Grasselly, vol. 3, 227–254. Budapest: Hungarian Academy of Sciences.

Winterhalter, B. 2004. "Ferromanganese Concretions in the Gulf of Bothnia." In *Mineral Resources of the Baltic Sea–Exploration, Exploitation and Sustainable Development. Zeitschrift Fur Angewandte Geologie*, special issue 2, edited by J. Harff, E. Emelyanov, M. Schmidt-Thome, and M. Spiridonov, 199–212. Hannover: Zeitschrift fur Angewandte Geologie.

Wu, Y.-H., L. Liao, C.-S. Wang, et al. 2013. "A Comparison of Microbial Communities in Deep-Sea Polymetallic Nodules and the Surrounding Sediments in the Pacific Ocean." *Deep-Sea Research Part I, Oceanographic Research Papers* 79: 40–49. https://doi.org/10.1016/j.dsr.2013.05.004.

Yli-Hemminki, P., K. S. Jørgensen, and J. Lehtoranta. 2014. "Iron–Manganese Concretions Sustaining Microbial Life in the Baltic Sea: The Structure of the Bacterial Community and Enrichments in Metal-Oxidizing Conditions." *Geomicrobiology Journal* 31: 263–275. https://doi.org/10.1080/01490451.2013.819050.

Yu, C., S. Turner, S. Huotari, et al. 2024. "Manganese Cycling and Transport in Boreal Estuaries Impacted by Acidic Mn-Rich Drainage." *Geochimica et Cosmochimica Acta* 365: 136–157. https://doi.org/10.1016/j.gca.2023.12.004.

Yu, C., J. J. Virtasalo, T. Karlsson, et al. 2015. "Iron Behavior in a Northern Estuary: Large Pools of Non-Sulfidized Fe(II) Associated With Organic Matter." *Chemical Geology* 413: 73–85. https://doi.org/10.1016/j.chemgeo.2015.08.013.

Zemskaya, T. I., A. V. Lomakina, E. V. Mamaeva, et al. 2018. "Composition of Microbial Communities in Sediments From Southern Baikal Containing Fe/Mn Concretions." *Microbiology* 87: 382–392. https://doi.org/10.1134/S0026261718030165.

Zhamoida, V., A. Grigoriev, K. Gruzdov, and D. Ryabchuk. 2007. "The Influence of Ferromanganese Concretions-Forming Processes in the Eastern Gulf of Finland on the Marine Environment." *Special Paper—Geological Survey of Finland* 45: 21–32.

Zhamoida, V., A. Grigoriev, D. Ryabchuk, et al. 2017. "Ferromanganese Concretions of the Eastern Gulf of Finland—Environmental Role and Effects of Submarine Mining." *Journal of Marine Systems* 172: 178–187. https://doi.org/10.1016/j.jmarsys.2017.03.009.

Zhamoida, V. A., W. P. Butylin, G. P. Glasby, and I. A. Popova. 1996. "The Nature of Ferromanganese Concretions From the Eastern Gulf of Finland, Baltic Sea." *Marine Georesources & Geotechnology* 14: 161–176. https://doi.org/10.1080/10641199609388309.

Zhang, F. S., C. Y. Lin, L. Z. Bian, G. P. Glasby, and V. A. Zhamoida. 2002. "Possible Evidence for the Biogenic Formation of Spheroidal Ferromanganese Concretions From the Eastern Gulf of Finland, the Baltic Sea." *Baltica* 15: 23–29.

Zhang, W., Y. Liu, and W. Zhao. 2023. "Occurrence and Enrichment of Cobalt in Ferromanganese Nodules From the Western Pacific." *Ore Geology Reviews* 163: 105758. https://doi.org/10.1016/j.oregeorev.2023.105758.

Supporting Information

Additional supporting information can be found online in the Supporting Information section.

14724669, 2025, 1, Downloaded from https://onlinelibrary.wiley.com/doi/10.1111/gbi.70010 by Luonnonvarakeskus, Wiley Online Library on [27/03/2026]. See the Terms and Conditions (https://onlinelibrary.wiley.com/terms-and-conditions) on Wiley Online Library for rules of use; OA articles are governed by the applicable Creative Commons License